Local moment approach as a quantum impurity solver for the Hubbard model

Himadri Barman*

Department of Theoretical Physics, Tata Institute of Fundamental Research, Homi Bhabha Road, Navy Nagar, Mumbai 400005, India

(Received 28 April 2015; published 5 July 2016)

The local moment approach (LMA) has presented itself as a powerful semianalytical quantum impurity solver (QIS) in the context of the dynamical mean-field theory (DMFT) for the periodic Anderson model and it correctly captures the low-energy Kondo scale for the single impurity model, having excellent agreement with the Bethe ansatz and numerical renormalization group (NRG) results. However, the most common correlated lattice model, the Hubbard model, has not been explored well within the LMA+DMFT framework beyond the insulating phase. Here in our work, within the framework we complete the filling-interaction phase diagram of the single band Hubbard model at zero temperature. Our formalism is generic to any particle filling and can be extended to finite temperature. We contrast our results with another QIS, namely the iterated perturbation theory (IPT) and show that the second spectral moment sum rule improves better as the Hubbard interaction strength grows stronger in LMA, whereas it severely breaks down after the Mott transition in IPT. For the metallic case, the Fermi liquid (FL) scaling agreement with the NRG spectral density supports the fact that the FL scale emerges from the inherent Kondo physics of the impurity model. We also show that, in the metallic phase, the FL scaling of the spectral density leads to universality which extends to infinite frequency range at infinite correlation strength (strong coupling). At large interaction strength, the off half-filling spectral density forms a pseudogap near the Fermi level and filling-controlled Mott transition occurs as one approaches the half-filling. As a response property, we finally study the zero temperature optical conductivity and find universal features such as absorption peak position governed by the FL scale and a doping independent crossing point, often dubbed the *isosbestic point* in experiments.

DOI: 10.1103/PhysRevB.94.045106

I. INTRODUCTION

The Hubbard model (HM) [1] is the simplest model that incorporates the on-site correlation effect between electrons in a lattice. Despite its appealing simplicity and applicability to Mott metal-to-insulator transition (MIT) [2], and high-temperature superconductivity [3], the model has remained a daunting challenge to the condensed matter physicists. It has been studied extensively from many angles including mean-field analytics and exact diagonalization numerics [4,5]. During the past decades, the dynamical mean-field theory (DMFT) has exhibited itself as an extremely powerful numerical method that simplifies the lattice model problem by mapping onto an effective interacting single impurity problem self-consistently connected to a fermionic bath via a hybridization function [6]. The mapping becomes exact at the infinite coordination number of the lattice and the self-energy becomes momentum independent at that limit. Even after the advent of the DMFT, solving an interacting lattice model remained elusive at the level of the effective impurity model problem. Therefore apart from the challenges that arise due to additional complication of a model (e.g., multiple orbitals, spin-orbit interaction, electron-phonon coupling, etc.), finding a suitable quantum impurity solver (QIS) for the DMFT method is still an ongoing issue. In addition to this, a quick or computationally less expensive QIS is required for systems having multiple bands, multiple layered structures, finite cluster sizes, and consisting of other real material-based parameters. In fact, besides the holy grail of getting the most accurate QIS, a race has began towards achieving the fastest QIS, which can at least capture the qualitatively correct physics and energy scales associated with it [7,8].

Depending on the invention of several QISs we may divide the DMFT timeline into two major decades starting from the early nineties. At the first decade several methods came up as candidates of the QIS, such as the iterated perturbation theory (IPT) [9–12], exact diagonalization (ED) [13], Hirsch-Fye quantum Monte Carlo (HFQMC) [11,14,15], noncrossing approximation (NCA) [16], and numerical renormalization group (NRG) [17,18]. All these methods could successfully capture the Mott MIT signaled by opening of a gap at the Fermi level of the spectral density. However, all of them suffer from limitations. For instance, ED exhausts the computational limit before one achieves a reasonable size of a lattice; HFQMC becomes disadvantageous at low temperature and suffers from the fermion sign problem [19]; NCA is only reliable for the insulating solution as the metal fails to promise a Fermi liquid; NRG becomes less accurate towards the high-energy (Hubbard bands) regime. Moreover, both ED and NRG suffer from energy discretization artifacts [20].

In the next decade, density-matrix renormalization group (DMRG) [21], dynamical density-matrix renormalization group (DDMRG) [22,23], fluctuation exchange approximation (FLEX) [24], and comparatively more recently the continuous time quantum Monte Carlo (CTQMC) [25–28] came up. FLEX becomes limited to a certain range of interaction strength [29]. On the other hand, although CTQMC can promise to work at very low temperature, it requires analytical continuation in order to get physical quantities in real frequency and the method of doing so is tedious and introduces additional errors [30]. Moreover, ED, DMRG, and CTQMC methods all demand expensive computational challenges.

*hbarhbar@gmail.com

Therefore if we just want to seek a semianalytical method, apart from the IPT and the NCA, another QIS, namely the local moment approach (LMA) deserves attention. LMA was pioneered by Logan and his co-workers at the end of the first decade and it became very efficient in capturing the low-energy Kondo scale in the single-impurity Anderson model (SIAM), and its strong-coupling behavior (infinite Hubbard interaction) shows excellent agreement with the Bethe ansatz [31] and NRG results [32]. Within the DMFT framework, LMA has been extensively applied to the particle-hole symmetric and asymmetric periodic Anderson model (PAM) that corresponds to Kondo insulators and heavy fermionic systems, respectively. In both cases the strong coupling (Kondo lattice limit) behavior of the low-energy scale has been captured well, and additionally the finite temperature transport and optical properties can explain many universal features found in experiments [33–37]. A recent study has exhibited how doping leads to mix valence to Kondo lattice crossover, in accord with such signatures found in transport and optical properties of several heavy fermion compounds [38]. In spite of all these successes, the Hubbard model has received less attention from the LMA aspect. Only the results of half-filling HM at large interaction have been reported, where LMA finds insulating spectral density for both the paramagnetic and antiferromagntic cases, and the strong-coupling Heisenberg (t-J) limit is captured correctly [39,40].

Here we extend the scenario for all interaction strengths and fillings. Recently a generic version of LMA with a variational method, called the variational LMA (VLMA) [41], was proposed for the multiorbital extension of the LMA. However, the method deviates from the conventional formalism, as already applied to SIAM and PAM, and does not ensure the Luttinger pinning (discussed in Sec. V) of the spectral density. In principle, our method could be applied to finite temperature as well, however, we restrict ourselves to the ground state only, leaving the finite temperature results a topic for a subsequent paper. We must mention another important concern of modern day QIS: the obedience of sum rules [20,42–44], e.g., whether the spectral moments from the numerics become closer to their exact values (details are discussed in the Sec. III). We discuss this aspect in the LMA case and show that the stronger the interaction, the spectral moment becomes more accurate.

Our work is organized as follows. In Sec. II we first describe the formalism for the half-filling, i.e., particle-hole (p-h) symmetric case, then we discuss the modification over it to deal with the asymmetric case, which specifically incorporates the Luttinger's sum rule [45] in the formalism. Next in Sec. III we show the numerical results, viz. spectral densities and properties derived from them. In places where required, we compare our results with that from another semianalytical QIS, namely the IPT. First we discuss the Fermi liquid behavior and its universal features in the metallic phase and Mott transition that occurs when interaction strength crosses a critical value (Sec. III A). In the same subsection, we describe one remarkable observation: LMA obeys the spectral moment sum rule very accurately at strong interaction, whereas the sum rule breaks down sorely after the MIT in IPT. We make a separate subsection for the off half-filling case (Sec. III B), where we show similar Fermi liquid universality found in the spectral density in the presence of a pseudogap at strong interaction and near the Fermi level. We show the spectral density evolution with the occupancy and find the filling controlled Mott transition signaled by vanishing quasiparticle residue at the half-filling. As an end result, we discuss the universal features of the optical conductivity, namely the universal absorption peak position and filling independent universal crossing point. We devote Sec. IV for comparisons with other numerical methods, particularly NRG and DDMRG. Then we discuss the low quasiparticle residue issue of LMA and propose a few possible variants of the standard LMA in Sec. V, that can remedy the issue. Finally in Sec. VI, we make a short summary of our results and analysis and discuss a few possible future extensions of the problem presented in the paper.

II. FORMALISM

As a part of formal introduction and for future references in the discussion part, we first write down the single band Hubbard model Hamiltonian below:

$$\hat{H} = -\sum_{\langle ij\rangle,\sigma} t_{ij} c^{\dagger}_{i\sigma} c_{j\sigma} + (\epsilon_d - \mu)\sum_{i\sigma} c^{\dagger}_{i\sigma} c_{i\sigma} + U\sum_{i} \hat{n}_{i\uparrow}\hat{n}_{i\downarrow}, \tag{1}$$

where t_{ij} is the amplitude of hopping from site i to site j in a lattice ($\langle\ \rangle$ notation restricts hopping to nearest neighbor sites only), operator $c^{\dagger}_{i\sigma}$ creates and $c_{i\sigma}$ destroys an electron with spin σ at site i, respectively, ($\hat{n}_{\sigma} = c^{\dagger}_{i\sigma} c_{i\sigma}$), U is the strength of on-site local Coulomb interaction, ϵ_d is the orbital energy of electrons at each site, and μ is the chemical potential of the system. The LMA formalism is built up on the fact that the transverse spin-flip scattering can play a crucial role in determining the energy scale that governs the physics of correlated lattice models. Such a transverse spin-flip scattering process appears as a polarization propagator in the standard diagrammatic perturbation theory and the site-diagonal term can be mathematically written as a convolution integration of "bare" propagators $\mathcal{G}_{\sigma}$ [46],

$$\Pi^{0}_{\sigma\,-\sigma}(\omega) = \frac{i}{2\pi}\int_{-\infty}^{\infty} d\omega'\, \mathcal{G}_{-\sigma}(\omega')\,\mathcal{G}_{\sigma}(\omega'-\omega). \tag{2}$$

Here we consider $\mathcal{G}_{\sigma}$ to be the spin symmetry broken or *unrestricted* Hartree-Fock (UHF) propagator: $\mathcal{G}_{\sigma}(\omega) = 1/(\omega - \Sigma^{0}_{\sigma} - \Delta(\omega))$, where $\Sigma^{0}_{\sigma} = \epsilon_d - \mu + U\langle\hat{n}_{-\sigma}\rangle = \epsilon_d - \mu + \frac{U}{2}(n - \sigma m)$ is called the UHF self-energy, $n \equiv \sum_{\sigma}\langle\hat{n}\rangle = -\frac{1}{\pi}\mathrm{Im}\sum_{\sigma}\int_{-\infty}^{\infty} d\omega\, \mathcal{G}_{\sigma}(\omega)$, $m \equiv \sum_{\sigma}\sigma\langle n_{\sigma}\rangle = -\frac{1}{\pi}\mathrm{Im}\sum_{\sigma}\int_{-\infty}^{\infty} d\omega\,\sigma\,\mathcal{G}_{\sigma}(\omega)$, and $\Delta(\omega)$ is the Feenberg self-energy [47].

Similar polarization propagators appear also in the higher order terms of the perturbation series and a careful observation infers that the local (site diagonal) terms of all orders can be arranged in a geometric progression and hence the net polarization propagator $\Pi_{\sigma\,-\sigma}$ can be expressed as [40]

$$\Pi_{\sigma\,-\sigma}(\omega) = \Pi^{0}_{\sigma\,-\sigma}(\omega)/\big(1 - U\,\Pi^{0}_{\sigma\,-\sigma}(\omega)\big). \tag{3}$$

$\Pi_{\sigma\,-\sigma}$ is often termed the random phase approximation (RPA) polarization propagator. It leads to a dynamic self-energy contribution that can be expressed in terms of another

convolution integral [40]:

$$\Sigma_\sigma(\omega) = \frac{U^2}{2\pi i}\int_{-\infty}^{\infty} d\omega' \mathcal{G}_{-\sigma}(\omega-\omega')\,\Pi_{\sigma\,-\sigma}(-\omega') = \frac{U^2}{2\pi i}\int_{-\infty}^{\infty} d\omega' \mathcal{G}_{-\sigma}(\omega+\omega')\,\Pi_{\sigma\,-\sigma}(\omega'). \quad (4)$$

Thus collecting the static UHF part Σ_σ^0 as well, we obtain the total self-energy:

$$\Sigma_\sigma^{\rm tot}(\omega) = \Sigma_\sigma^0 + \Sigma_\sigma(\omega). \quad (5)$$

The two spin-dependent self-energies give rise to two interacting Green's function $G_\sigma = (\mathcal{G}_\sigma^{-1} - \Sigma_\sigma)^{-1} \equiv (\mathcal{G}^{-1} - \Sigma_\sigma^{\rm tot})^{-1}$, which is not directly useful in the case where spin symmetry is not actually broken (usual paramagnetic case). Therefore to calculate the impurity Green's function in the DMFT context, we find the spin-averaged Green's function,

$$G(\omega) = \tfrac{1}{2}(G_\uparrow(\omega) + G_\downarrow(\omega)), \quad (6)$$

and obtain a spin-independent self-energy by exploiting the Dyson's equation ($G^{-1} = \mathcal{G}^{-1} + \mu - \epsilon_d - \Sigma$):

$$\Sigma(\omega) = \frac{1}{2}(\Sigma_\uparrow^{\rm tot}(\omega) + \Sigma_\downarrow^{\rm tot}(\omega)) + \frac{\left[\frac{1}{2}(\Sigma_\uparrow^{\rm tot}(\omega) - \Sigma_\downarrow^{\rm tot}(\omega))\right]^2}{\mathcal{G}^{-1}(\omega) - \frac{1}{2}(\Sigma_\uparrow^{\rm tot}(\omega) + \Sigma_\downarrow^{\rm tot}(\omega))}, \quad (7)$$

where $\mathcal{G}$ is the host Green's function of DMFT's effective impurity model $\mathcal{G}(\omega) = 1/(\omega - \Delta(\omega))$ with $\Delta(\omega)$ playing the role of the hybridization function. Instead of using Eq. (7), which apparently looks cumbersome, we find Σ by writing

$$G(\omega) = \frac{1}{\gamma(\omega) - \Delta(\omega)};\ \gamma(\omega) \equiv \omega + (\mu - \epsilon_d) - \Sigma(\omega). \quad (8)$$

We similarly can express $G_\sigma(\omega) = 1/(\gamma_\sigma(\omega) - \Delta(\omega))$ with $\gamma_\sigma(\omega) \equiv \omega - \Sigma_\sigma^{\rm tot}(\omega)$ and then by exploiting Eq. (6) we determine

$$\gamma(\omega) = \frac{2\gamma_\uparrow(\omega)\gamma_\downarrow(\omega) - [\gamma_\uparrow(\omega) + \gamma_\downarrow(\omega)]\Delta(\omega)}{\gamma_\uparrow(\omega) + \gamma_\downarrow(\omega) - 2\Delta(\omega)}. \quad (9)$$

To attain the DMFT self-consistency on the lattice side, we find the local Green's function by performing the Hilbert transform: $G(\omega) = \int_{-\infty}^{\infty} d\epsilon\, D_0(\epsilon)/(\gamma(\omega) - \epsilon)$ for a given noninteracting lattice density of states (DoS) $D_0(\omega)$. Furthermore, for the metallic phase, in order to ensure the Fermi-liquid property ($\mathrm{Im}\Sigma(\omega) \propto (\omega - \mu)^2$), we add the following condition (often dubbed *symmetry restoration* in earlier literature) into the DMFT equations:

$$\sum_\sigma \sigma\,\Sigma_\sigma(0) = |m|\,U. \quad (10)$$

In the p-h symmetric case, we use the condition $\epsilon_d - \mu = -U/2$, where μ is chosen to be zero in practice. However, for the asymmetric case, we do not have such a simple relation between the orbital energy and the Coulomb interaction strength. Also there should be a shift $\delta\mu$ from the chemical potential μ, which is set to be zero in the symmetric case. Therefore the UHF Green's function gets modified as $\mathcal{G}_\sigma(\omega) = 1/[\omega^+ - \tilde{\epsilon} + \sigma|m|U/2 - \Delta(\omega)]$ where $\tilde{\epsilon} \equiv \epsilon - \delta\mu \equiv \epsilon_d - \mu + Un/2 - \delta\mu$ which is zero only in the half-filled case ($\epsilon = 0$, $\delta\mu = 0$).

Now there are two important algorithmic steps that are worth mentioning.

(i) We parametrize a quantity $x \equiv \frac{1}{2}|m|U$ and for a given x; we determine U by the Fermi liquid condition [Eq. (10)] for the metallic case. For the insulating case, this condition is not required, however, a pole arises at $\omega = 0$ in $\mathrm{Im}\Pi_{\sigma\,-\sigma}(\omega)$, which needs to be taken care by analytically adding its weight to the self-energy [40].

(ii) For the p-h asymmetric case, once we find U, we calculate $\Sigma(\omega)$ and $G(\omega)$ for a fixed $\tilde{\epsilon} = \epsilon_d - \mu + Un/2 - \delta\mu$, and then setting $\mu = 0$, we find ϵ_d by self-consistently satisfying Luttinger's sum-rule [45,48,49]:

$$\mathrm{Im}\int_{-\infty}^{\mu} d\omega\, G(\omega)\frac{\partial\Sigma(\omega)}{\partial\omega} = 0. \quad (11)$$

An asymmetry parameter $\eta \equiv 1 + 2\epsilon_d/U$ ($\mu = 0$) is introduced to quantify p-h asymmetry in our calculations. Note that for the symmetric case, $\epsilon_d = -U/2$ and hence $\eta = 0$.

III. RESULTS AND DISCUSSIONS

We separate our results and corresponding discussions into Sec. III A, the particle-hole symmetric or half-filling ($n = 1$) case, and Sec. III B, the case away from it ($n \neq 1$). Our discussions mostly comprise the properties of single-particle spectral density and analysis following those at different parameter regimes at zero temperature. Note that as a part of the DMFT method, the hopping amplitude in Eq. (1) is taken to be uniform and we define a new hopping amplitude t_* such that $t_{ij} = t_*/\sqrt{z}$, z being the coordination number. Throughout the paper we choose $t_* = 1$ for our calculation, and results are mainly discussed for the d-dimensional hypercubic lattice ($z = 2d$) although we mention results for the Bethe lattice explicitly where it is required (e.g., comparing with results from NRG calculations). The noninteracting DoS of the lattice is defined as $D_0(\omega) \equiv 1/(\sqrt{\pi}t_*)\exp(-\omega^2/t_*^2)$. At the end of Sec. III B, we keep a special subsection for the optical properties, for which we use the standard Kubo formula from the linear response theory [16,50].

A. Half-filling

1. *Universal scaling behavior of spectral density*

The key investigative question that arises at the half-filling case is whether the Mott transition is seen at large Coulomb interaction U, which should be reflected by formation of a gap at the Fermi level (set at $\omega = 0$ in our convention) in the spectral density, $D(\omega) = -\frac{1}{\pi}\mathrm{Im}G(\omega)$. Before we seek an answer, we first look at the low-energy behavior of the spectral density for small interaction strength U and hence for small x. Figure 1(a) shows the presence of finite DoS at the Fermi level in the form of quasiparticle or the Abrikosov-Suhl resonance, clearly signaling a metallic phase (The inset figure shows the usual three-peak full spectral density at various U/t_*'s.). We notice that all the resonance peaks are pinned at the noninteracting value at the Fermi level: $D(0) = D_0(0) = 1/\sqrt{\pi}$. This is known as the Luttinger

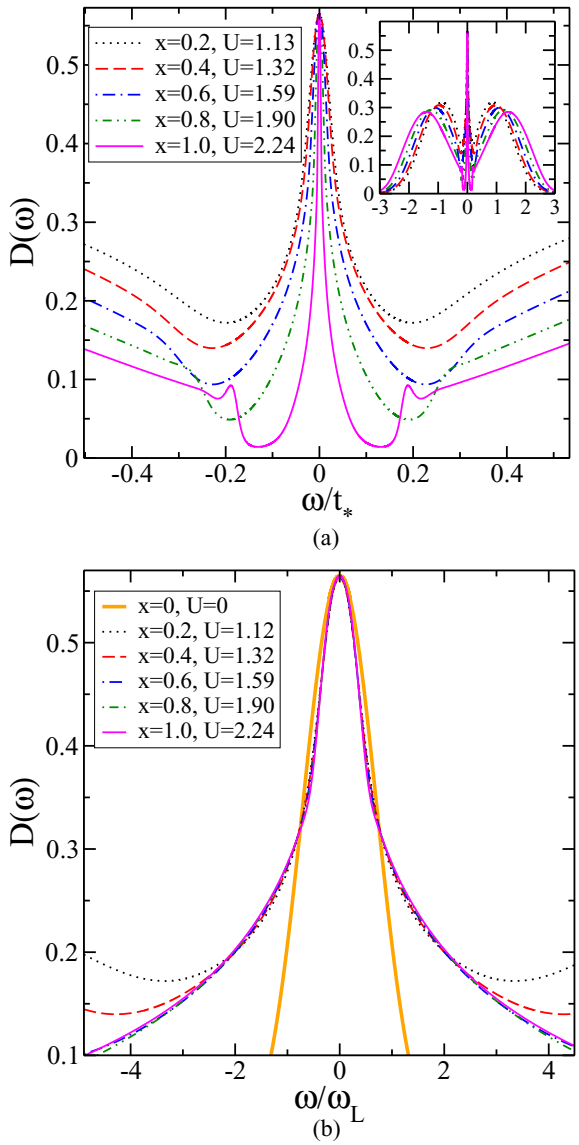

FIG. 1. Spectral densities and their scaling collapse. (a) Abrikosov-Suhl resonance appears at the Fermi level ($\omega = 0$) and the resonance width decreases with increasing x or U. (Inset) Full spectra for the same. (b) Scaling collapse of spectral densities when the frequency axis is scaled by the low-energy scale $\omega_L = Zt_*$. Note that the collapse deviates from the noninteracting curve ($U = 0$) almost immediately away from the Fermi level.

pinning [51], which is a direct consequence of the Luttinger's sum rule mentioned in the earlier section [45]. The resonance width shrinks gradually as we increase x or U, and we can associate an effective low-energy scale, $\omega_L = Zt_*$, determined from the quasiparticle residue $Z = 1/(1 - \partial_\omega \mathrm{Re}\Sigma(\omega)|_{\omega=0})$, proportional to the width of the resonance. From Fig. 1(b) we can see that all spectral densities collapse to a universal value around the Fermi level when we scale the frequency axis by ω_L. Nevertheless the collapsed spectral density seems to deviate from the noninteracting limit almost immediately away from the Fermi level. Thus, even though adiabatic continuity at the Fermi level is maintained in our formalism through satisfying Eq. (10), the renormalized noninteracting

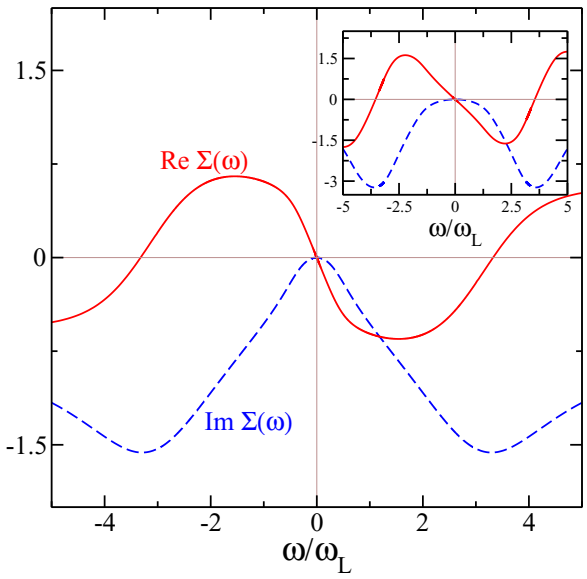

FIG. 2. Reason for noncollapse with the noninteracting DoS. Dashed lines (blue in color) and full lines (red in color) are the imaginary and real part of the self-energy, respectively. The static part $\Sigma(0) = U/2$ has been subtracted from the real part. $\mathrm{Im}\Sigma(\omega)$ grows far more rapidly from $\omega = 0$ in LMA (main panel) than that in IPT (inset) suggesting that not only in the strong coupling regime, but also in the intermediate correlation regime, incoherent scattering effects become important at energies even slightly away from the Fermi level. The interaction strength for the LMA, $U = 1.13t_*$ ($x = 0.2t_*$); for the IPT, $U = 3.0t_*$.

limit (RNIL) description is seen to be invalid. This can be explained if we look at the self-energy behavior at low frequency.

The RNIL assumes that contribution from $\mathrm{Im}\Sigma(\omega)$ is negligible compared to the contribution from $\mathrm{Re}\Sigma(\omega)$ at low ω since the former vanishes as $\omega \to 0$ with one power of ω ($\propto\omega^2$) higher than the latter ($\propto\omega$). This assumption does hold in IPT over a large interval around the Fermi level. However, the contributions from both the real and imaginary parts of $\Sigma(\omega)$ become comparable when the coefficient of the imaginary part becomes large enough. Figure 2 shows that the slope change in $\mathrm{Im}\Sigma(\omega)$ away from $\omega = 0$ is faster in LMA (shown in the main panel) compared to that in IPT (shown in the inset). Nevertheless the scaling collapse and Luttinger pinning of the spectral density ensure the Fermi liquid nature of the metallic phase in LMA.

2. *Emergence of low-energy scale in susceptibility*

Since spin-flip scattering is responsible for the rise of the Kondo energy scale of an impurity model and the impurity physics persists in a lattice through the self-consistency of the DMFT formalism, it is natural to intuit such a scale in LMA. Moreover, in the strong-coupling Kondo regime (Fermi liquid) the Kondo scale should be proportional to $\omega_L = Zt_*$ [52]. The bottom inset of Fig. 3 shows that $\mathrm{Im}\Pi_{\sigma-\sigma}(\omega)$ has a maximum or peak at $\omega = \omega_m$. Once we scale the frequency axis by ω_L (main panel of Fig. 3), the positions of those peaks fall at the same value, which clearly indicates a proportional

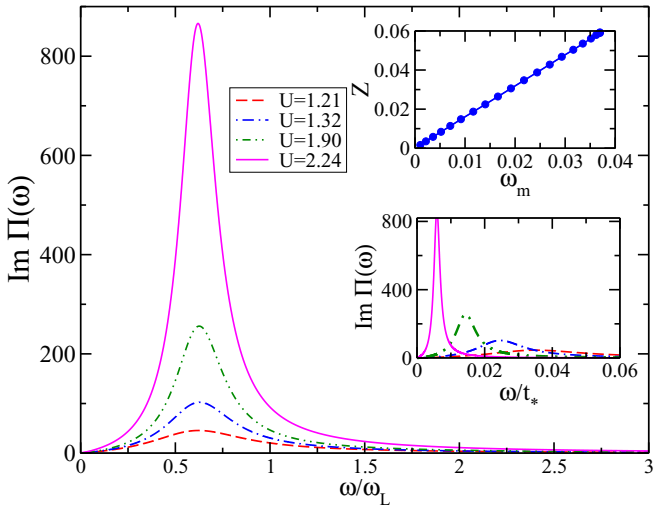

FIG. 3. (Bottom inset) The peak position of $\mathrm{Im}\Pi_{\sigma-\sigma}(\omega)$ gives rise to an energy scale ω_m for various U's. (Main panel) The position becomes universal when the frequency is scaled by $\omega_L = Zt_*$ signifying a proportional relation between Z and ω_m. (Top inset) Z vs ω_m plot is a nice straight line with slope 1.59.

relation between ω_m and the Fermi liquid scale ω_L. The presence of such maxima gives rise to maxima in response functions such as the imaginary part of spin susceptibility and absorption spectrum (real part of dynamic conductivity). Recent DMFT studies using various impurity solvers have shown that indeed the position of the imaginary part of local spin susceptibility becomes universal while the frequency axis is scaled by ω_L [53]. The top inset of Fig. 3 reaffirms our statement showing a linear dependence of Z on ω_m with a slope 1.59 (proportionality constant).

3. *Mott transition and presence of hysteresis*

It has already been mentioned that the width of the quasiparticle resonance in the spectral density shrinks gradually as U/t_* is increased, which disappears finally by opening up a gap at the Fermi level. Thus our primary question is answered and indeed an interaction-driven MIT, i.e., Mott transition occurs when interaction strength is greater than a critical value, i.e., $U \geqslant U_{c2}$. For the hypercubic lattice, we find approximately $x_{c2} = 1.2t_*$ which implies $U_{c2} \simeq 2.64t_*$. This value is close to the analytically estimated value $2.69t_*$ (see Appendix). In the main panel of Fig. 4 we see that a gap opens at the Fermi level in the spectral density at $U = 3.56t_*$. The estimation of U_{c2} is carried out through an extrapolation of the zero crossing of the low-energy scale ω_L with increasing U (see line with open circles in Fig. 5). In IPT, it has been seen [50], in the zero temperature evolution of spectral densities with interaction strength, that there exist two transition points U_{c1} and U_{c2} depending on whether we are changing U from the metallic or insulating side. Therefore it is natural to ask: If we start from an insulating regime and keep on decreasing x (hence U), do we get an insulator to metal transition at the same point that we have mentioned above? The right inset of Fig. 4 shows that we find that the gap decreases as we decrease x from $2.0t_*$ ($U = 4.13t_*$) and it appears that the gap closes at $x \sim 1.06t_*$, i.e., $U = 2.38t_*$. However, the gap

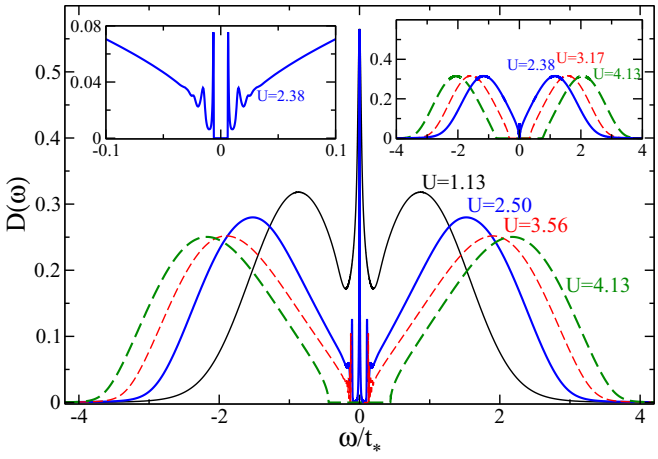

FIG. 4. Mott transition reflected from the spectral density evolution as U changes at zero temperature (for the hypercubic lattice). (Main panel) Quasiparticle resonance shrinks as U is increased. At $U = 3.56t_*$, a clear gap opens up at the Fermi level signaling the Mott metal-to-insulator transition (MIT). The gap gets enhanced as U is increased further. (Right panel) Starting from a Mott insulator if U is decreased, the gap at the Fermi level decreases and eventually closes at $U < 2.38t_*$. (Left panel) A finite gap still persists at $U = 2.38t_*$. Therefore an extrapolation method is required to find the critical value U_{c1} where insulator-to-metal transition (IMT) happens (see Fig. 5).

is truly not zero at $U = 2.38t_*$ as the left inset of Fig. 4 shows in a zoomed view. For this reason we plot the gap (Δ_g) as a function of U/t_* in Fig. 5 (dashed line with open squares). We find that Δ_g almost linearly decreases with U/t_* and to our estimation $U_{c1} \simeq 2.36t_*$. Thus similar to the IPT result, LMA

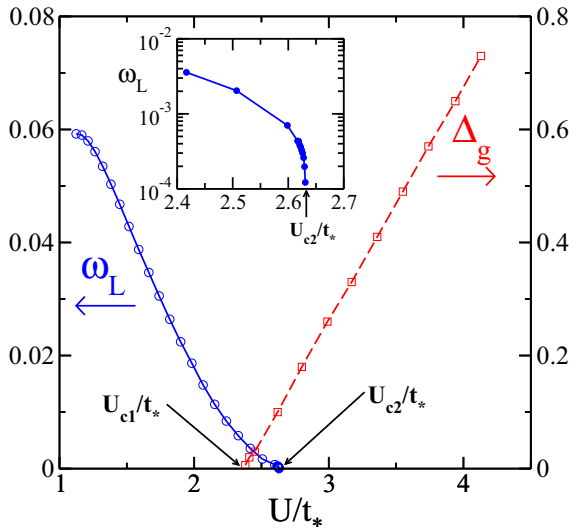

FIG. 5. Decay of the low-energy scale $\omega_L = Zt_*$ with increasing U/t_* (solid line). Inset shows the same in log scale. ω_L seems to vanish at $U_{c2} = 2.64t_*$. Note that we have been able to reach a value of the low-energy scale $\sim 10^{-4}t_*$, which requires very high precision calculations. The dashed line shows that the spectral gap Δ_g of the Mott insulator decreases linearly with decreasing U/t_* and closes at $U_{c1} = 2.36t_*$.

also shows the presence of a coexistence regime (possibility of having both metallic and insulating solutions) and hence hysteresis driven by interaction. The width of the coexistence regime, i.e., $\Delta U_c \equiv U_{c2} - U_{c1}$ is $0.28t_*$ for the hypercubic lattice, which is quite less than that found in IPT ($\Delta U_c \sim 0.7t_*$) [50]. In Bethe lattice the coexistence regime is further small ($U_{c2} \simeq 3.5t_*$ and $U_{c1} = 3.4t_*$ for bandwidth $4t_*$) and thus a question remains open: Does interaction-driven hysteresis indeed occur in LMA or is it due to an artifact of the numerical limitation?

4. Spectral moment sum rules

Spectral moments are often considered to be important in testing the robustness of a certain numerical or analytical method for a many-body problem [42,54]. An mth spectral moment is defined as $M_m \equiv \int_{-\infty}^{\infty} d\omega\, \omega^m D(\omega)$, which at the same time, can be exactly evaluated from a model Hamiltonian using the equation of motion method: $M_m = \langle\{\mathcal{L}^n d_\sigma, d_\sigma^\dagger\}\rangle$ with $\mathcal{L}\mathcal{O} = [\mathcal{O},\mathcal{H}]$, $\mathcal{L}^2\mathcal{O} = [[\mathcal{O},\mathcal{H}],\mathcal{H}]$, so on. $M_0 = 1$ is true for any model and for the Hubbard model one can find: $M_1 = \epsilon_d - \mu + U\langle n_\sigma\rangle$, $M_2 = \sum_{\mathbf{k}} \epsilon_{\mathbf{k}}^2 + (\epsilon_d - \mu)^2 + U\langle n_\sigma\rangle[2(\epsilon_d - \mu) + U]$, $M_3 = M_1 M_2$. Here $\epsilon_{\mathbf{k}}$ is the dispersion of the given lattice whose momentum ($\mathbf{k}$) sum is nothing but the second spectral moment of the noninteracting DoS, i.e., $\sum_{\mathbf{k}} \epsilon_{\mathbf{k}}^2 = M_2^0 \equiv \int_{-\infty}^{\infty} d\omega\, \omega^2 D_0(\omega)$. For instance, for a Bethe lattice DoS, $D_0(\omega) \equiv \frac{1}{2\pi t_*^2}\sqrt{4t_*^2 - \omega^2}$, $M_2^0 = t_*^2$, and for our hypercubic lattice DoS, $M_2^0 = \frac{1}{2}t_*^2$. For the half-filling case, we obtain further simplification: $M_1 = 0$, $M_2 = M_2^0 + U^2/4$, $M_3 = 0$. Now in the IPT calculation, the relative errors in M_1 and M_3 vary within the order 10^{-3}–10^{-5} and 10^{-2}–10^{-3}. On the other hand, in LMA, the error goes to the order of 10^{-10}–10^{-12} as one approaches towards higher U. In the half-filling case, specifically the second moment M_2 becomes very crucial. Figure 6(a) shows that numerically calculated M_2 significantly agrees with the expected analytical value, however, the agreement severely breaks down in the insulating regime in IPT ($U > U_{c2} = 4.4t_*$). On the contrary, in LMA, the agreement is comparatively poor in the metallic side, but the difference (ΔM_2) between the exact and numerical values decreases as U increases and it appears that $\Delta M_2 \to 0$ as $U \to \infty$ [see Fig. 6(b)]. The absolute values of the relative errors are shown in the insets. A very recent paper [44] has reported higher accuracy in the spectral moments up to the third order using a new alternative diagonalization-based QIS. Nevertheless the method is heavily expensive in computation time and limited by a finite number of sites, and errors could be introduced by the broadening over discretization, which fails to ensure the Luttinger pinning at the Fermi level.

5. Strong correlation universality

As noticed in Fig. 1(b), the spectral density seems to assume a universal form $D(\omega) = D(\omega/\omega_L)$ leading to collapse of $D(\omega)$ up to a certain frequency range. As U/t_* increases, this range keeps on increasing and close to the Mott transition, we find scaling collapse in the spectral densities for decades of ω_L (see main panel of Fig. 7: U ranging from $2.07t_*$ to $2.60t_*$), when the frequency axis is scaled by the same energy scale. Moreover, this universal regime extends to higher and higher

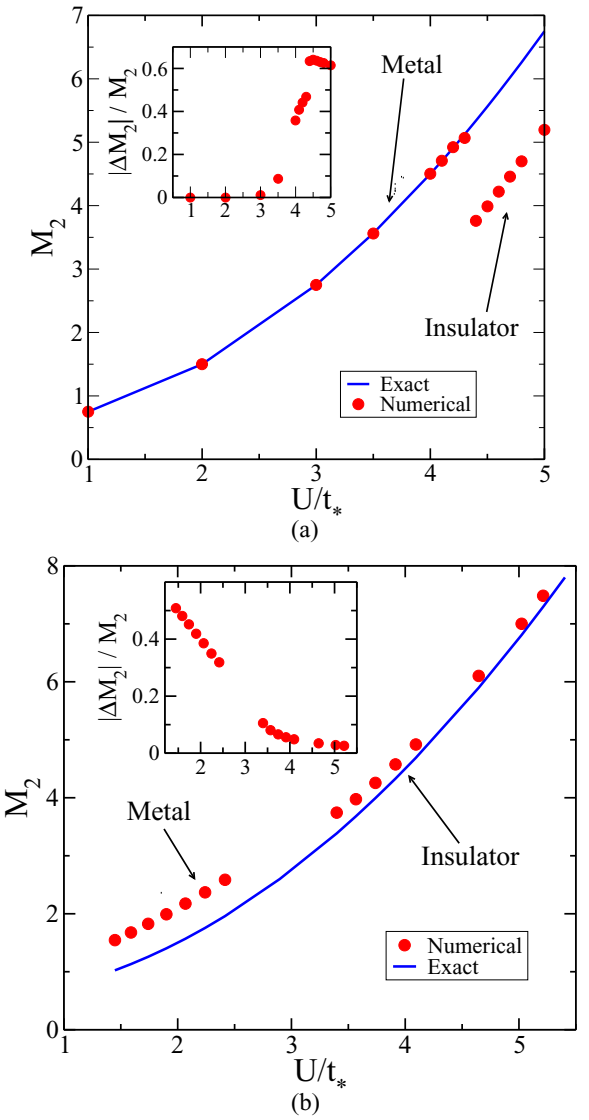

FIG. 6. Second spectral moment M_2 in (a) IPT and (b) LMA for various interaction strengths. The insets show the respective absolute values of relative error.

frequencies as we increase U/t_* suggesting that in the limit $U \to U_{c2}^-$, the universal scaling region extends to all the way until the frequency reaches one of the Hubbard bands. The universal scaling form is seen to be very different from the RNIL suggesting very nontrivial tails of the spectral function for large ω/ω_L. These tails should manifest themselves in transport and other finite temperature/frequency properties that would be an interesting feature to look for in experiments [34].

B. Away from half-filling

1. Spectral density: empty orbital, mixed valence, and doubly occupied orbital states

Before we embark on the results, we first make a few qualitative remarks. When the electron density is not equal to one per site, i.e., away from the half-filling, there are always empty sites available for electrons/holes to hop without

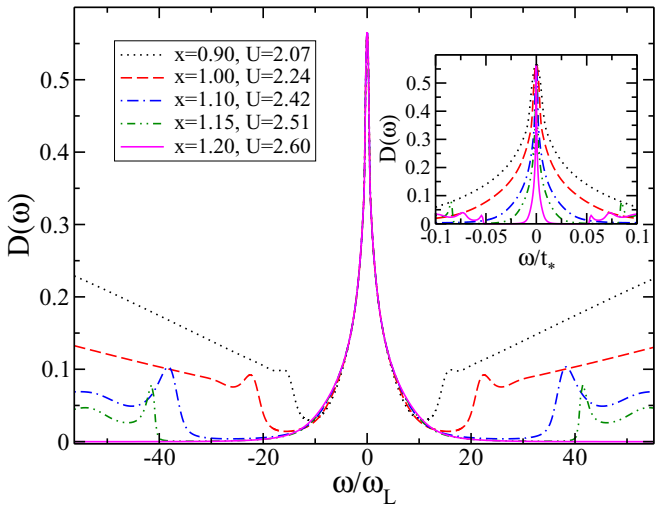

FIG. 7. Scaling universality at strong correlation strength: As $U \to U_{c2}^{-}$, the collapse of the spectral density extends all the way after the frequency being scaled by ω_L, despite being limited to the low-energy scale regime, which could be order of ω_L. For example, the scaling agreement between spectral densities at $U = 2.51t_*$ and $U = 2.60t_*$ runs up to $\sim 30\omega_L$. The inset shows the same spectral densities without the scaling.

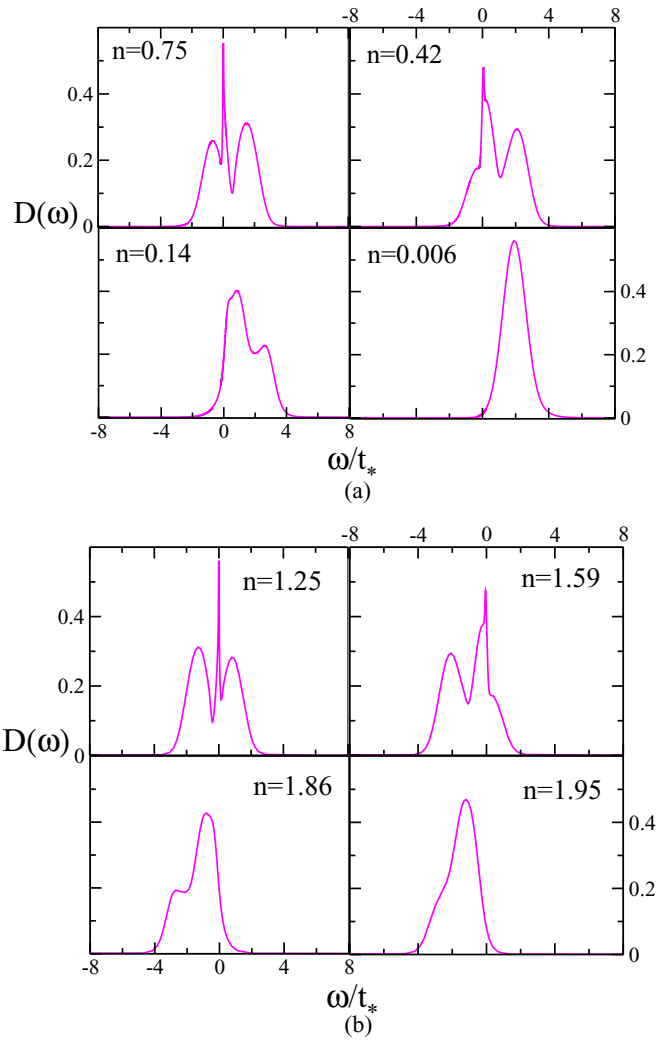

FIG. 8. Evolution of spectral densities for $x = 0.5t_*$ ($U \simeq 1.5t_*$) at $n \neq 1$ (away from half-filling), for the hypercubic lattice. Parent (half-filled, i.e., $n = 1$) phase is metallic. (a) Evolution from $n \leqslant 1$ to $n \to 0$. (b) Evolution from $n \geqslant 1$ to $n \to 2$.

encountering the Coulomb repulsion U. Therefore we can get Mott insulators only when the filling reaches the half-filled value ($n = 1$). However, there can be special situations, namely $n = 2$ where electron's hopping is forbidden since orbitals at all sites are fully (doubly) occupied. This leads to an insulator, which is in fact a band insulator. Similarly for the $n \to 0$ case, there will be only a few electrons left for conduction, or from the hole point of view, the sites will be fully occupied by holes and will lead to a band insulator again. Thus at zero temperature we can divide the n space into five distinct regimes, viz. (i) empty orbital ($n \to 0$), (ii) mixed valence-I ($0 < n < 1$), (iii) symmetric metal or Mott insulator ($n = 1$), (iv) mixed valence-II ($1 < n < 2$), and (v) doubly occupied orbital ($n \to 2$). The regimes (iv) and (v) are p-h symmetric counterparts of (ii) and (i), respectively. Figures 8(a) and 8(b) show the evolution of spectral density towards the two extremes [regime (i) and regime (v)] for the hypercubic lattice, starting from a half-filled Fermi liquid metal ($n = 1$). In the first case, the lower Hubbard band starts moving towards the Fermi level ($n = 0.75$) with decreasing its height compared to the upper Hubbard band, then it coalesces with the quasiparticle resonance ($n = 0.42$) where resonance itself shifts away from the Fermi level. Gradually the lower Hubbard band and the qausiparticle features do not remain significant any more ($n = 0.14$) and the density just behaves like a noninteracting one, situated above the Fermi level, thus being a band insulator with the band edge at the Fermi level. Similarly in the second case, the upper Hubbard band moves towards the Fermi level and finally the lower Hubbard band occupies the whole spectral region and the system becomes an empty orbital band insulator [regime (i)]. Thus Figs. 8(a) and 8(b) reflect the fact that a particle with $1 \leqslant n \leqslant 2$ has its hole counterpart in $0 \leqslant n \leqslant 1$. A schematic phase diagram on the occupancy-interaction plane at zero temperature is shown in Fig. 9(a). The filling control MIT can be inferred by looking at quasiparticle residue Z, as it continuously vanishes at the half-filling ($n = 1$). Figure 9(b) shows this behavior for both LMA (main) and IPT (inset), where Z only differs by an order of magnitude.

2. *Pseudogap formation and strong-coupling universality*

The main panel of Fig. 10 shows that after certain U/t_* ($\sim 2.7t_*$) a pseudogap starts to form near the Fermi level (*pseudo* since the gap does not open exactly at the Fermi level). The gap increases as we increase U/t_* further. We notice that the pseudogap has the same width as the gap in the Mott insulator has in half-filling. It seems that the quasiparticle weight never vanishes at any large finite U/t_* above U_{c2}/t_* and hence the pseudogap never touches (however close it may be) the Fermi level. This is expected because once we go away from half-filling, even by infinitesimal doping, we never expect a Mott transition. The pseudogap feature, however, is not observed using IPT [55]. Therefore, the feature might be

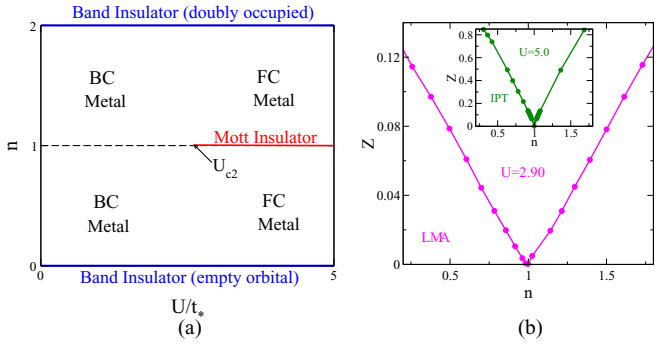

FIG. 9. (a) Phase diagram on the occupancy-interaction (n-U) plane. The region is bounded along the filling axis by empty orbital and doubly occupied band insulator lines. The metal emerging by doping a Mott insulator side is known as the filling controlled (FC) metal ($U > U_{c2}$) and remaining region is the bandwidth controlled (BC) metal since interaction is low. In case of LMA, $U_{c2} = 2.64t_*$. (b) Disappearance of quasiparticle residue Z as occupancy approaches the half-filling value $n = 1$ in IPT (inset, $U = 5.0t_*$) and LMA (main, $U = 2.9t_*$).

tied to the transverse spin-flip scattering process inherent in LMA.

Similar to the half-filled case, the scaling universality for strong interaction strength extends to very large frequencies beyond the low-energy Fermi liquid scale ω_L (see inset of Fig. 10) and it appears that as we increase U/t_* further, the scaling agreement extends further and at strong-coupling limit ($U \to \infty$), we expect the scaling universality will extend all the way in frequency, i.e., up to $\omega/\omega_L \to \pm\infty$, since the Hubbard bands are positioned at $\pm\infty$ now.

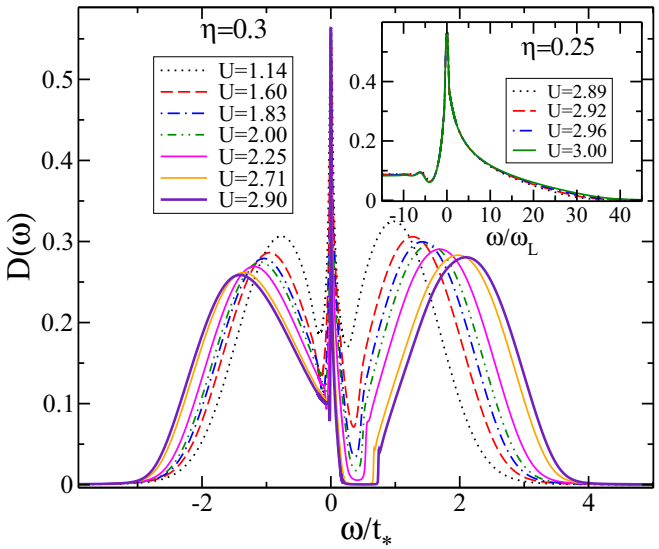

FIG. 10. (Main) Spectral densities at various U/t_*'s at asymmetry parameter $\eta = 0.3$. A pseudogap (a gap close to the Fermi level) forms in the spectral density at $U = 2.9t_*$. (Inset) Scaling universality at strong interaction values at $\eta = 0.25$: $U/t_* = 2.89$, 2.92, 2.96, and 3.00. The universal region extends to very large values of ω/ω_L and the universal scaling form is seen to be very different from the renormalized noninteracting Gaussian form.

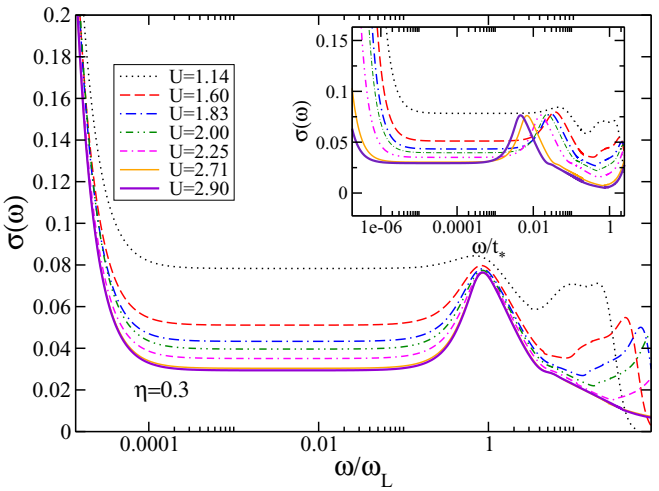

FIG. 11. Scaling behavior in the optical conductivity $\sigma(\omega)$ for the asymmetry parameter $\eta = 0.3$ and different interaction strengths. The first absorption peaks arise at $\omega = \omega_L$ (inset), as revealed from the scaling of the frequency axis by ω_L, leaving all peaks appearing at $\omega/\omega_L = 1$ (main).

3. *Optical conductivity*

Carrying a motivation to derive some physical properties out of our zero temperature spectral densities, we seek the optical properties. Being doped and hence metallic in nature, a divergent Drudé peak appears at $\omega = 0$ of the optical conductivity $\sigma(\omega)$, accompanied by an absorption peak positioned at $\omega = \omega_L$ (see inset of Fig. 11, Drudé peaks are out of scale). This uniqueness of the peak position becomes evident when we divide the frequency axis by corresponding ω_L for various U/t_*'s at fixed asymmetry parameter η. For instance, at $\eta = 0.3$ all of the first absorption peak of $\sigma(\omega)$ for different U/t_*'s, arise at $\omega/\omega_L = 1$ (see main panel of Fig. 11). This result is very significant because any experimental probe that finds the absorption spectra of a material in a certain condition, can easily determine the associated low-energy scale of it by looking at the position of the first absorption peak. Moreover, this universal feature of the absorption peaks implies that such a universality is merely a signature of a Fermi liquid and does not get affected by doping as long as the phase remains a Fermi liquid. Another interesting feature is noticed when the optical conductivity is computed for different hole dopings $\delta \equiv 1 - n$, keeping the interaction unchanged. The main panel of Fig. 12 depicts $\sigma(\omega)$ at various dopings (δ ranging from 0 to 0.25) where we notice that a universal crossing point appears around $\omega \simeq t_*$. This behavior does indeed bear close similarity to the experiments on compounds of the formulas $R_{1-x}Ca_xTiO_{3+y}$, R representing rare-earth metals, done by Katsufuji *et al.* [56] (see inset of Fig. 12). Similar spectral weight transfer through a universal point or a pointlike region in the cuprates (e.g., $La_{2-x}Sr_xCuO_x$ [57] and $Pr_{2-x}Ce_xCuO_4$ [58]), Sr doped $LaCoO_3$ [59], and very recently in $NiS_{2-x}Se_x$ [60] has been observed. Such a universal point is termed the *isosbestic point* and presence of it is often considered to be reminiscence of the correlation effect [61,62].

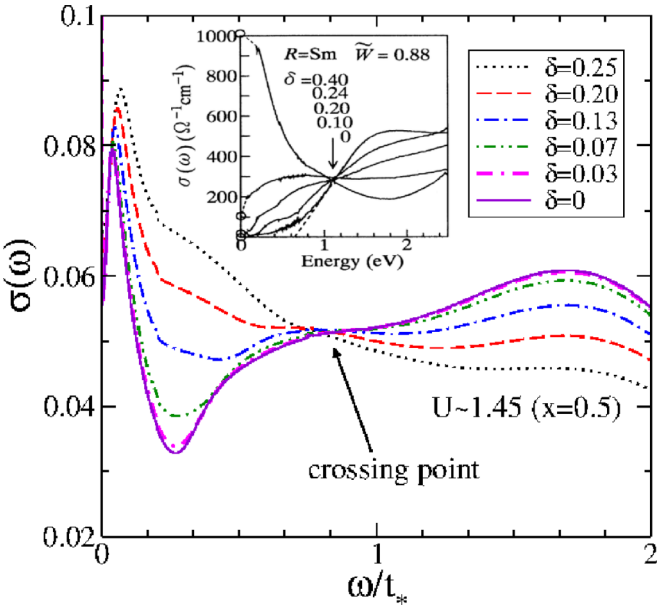

FIG. 12. (Main) LMA results for optical conductivity with various hole concentrations: $\delta = 1 - n$. (Inset) Optical conductivity for $Sm_{1-x}Ca_xTiO_3$ where $\tilde{W}$ is the bandwidth obtained from a tight-binding calculation, mentioned in Ref. [56], normalized to that of $LaTiO_3$.

IV. COMPARISONS TO OTHER METHODS

It is evident in Fig. 9(b) that the value of Z is one order of magnitude less compared to that in IPT at U/t_* of the same order. However, the essential physics does not alter much (e.g., Fermi liquid properties of the metallic phase, bandwidth, and filling controlled Mott transition). Now when we scale the frequency by the FL scale ω_L, we find excellent agreement with NRG spectral density up to $\sim 2\omega_L$ in the p-h symmetric case, while the IPT spectral density deviates from the NRG immediately after the Fermi level [main, Fig. 13(a)] [63]. In the p-h asymmetric case, the agreement between scaled NRG and LMA spectral densities continues beyond $\sim 2\omega_L$ and stops almost at the onset of the Hubbard bands [inset, Figure 13(a)]. It is needless to say that one should not expect the agreement in the Hubbard bands during such low-energy scaling of spectral densities. The scaling agreement indicates that the spin-flip dynamics incorporated in LMA, missed in IPT, indeed captures the same Kondo scale physics, in parallel with the agreement already found in the single impurity and pseudogap Anderson models [32,64,65].

We also compare the closing of the Mott gap with various other methods. Figure 13(b) shows that the Mott gap Δ_g diminishes with decreasing U/t_* in the insulating regime and finally closes at $U = U_{c1}$. Although U_{c2} differ significantly, as mentioned in [41] for the Bethe lattice of bandwidth (BW) $2t_*$, U_{c1} in LMA and VLMA are quite close ($1.45t_*$ and $1.6t_*$, respectively) and they differ a little in the gap size. The Δ_g vs U/t_* curve behaves almost linearly for LMA and strong-coupling perturbation theory (SCPT) by Eastwood *et al.* [66], whereas the curve for IPT and DDMRG by Karski *et al.* [23] show almost identical nonlinear power-law-like behavior [23].

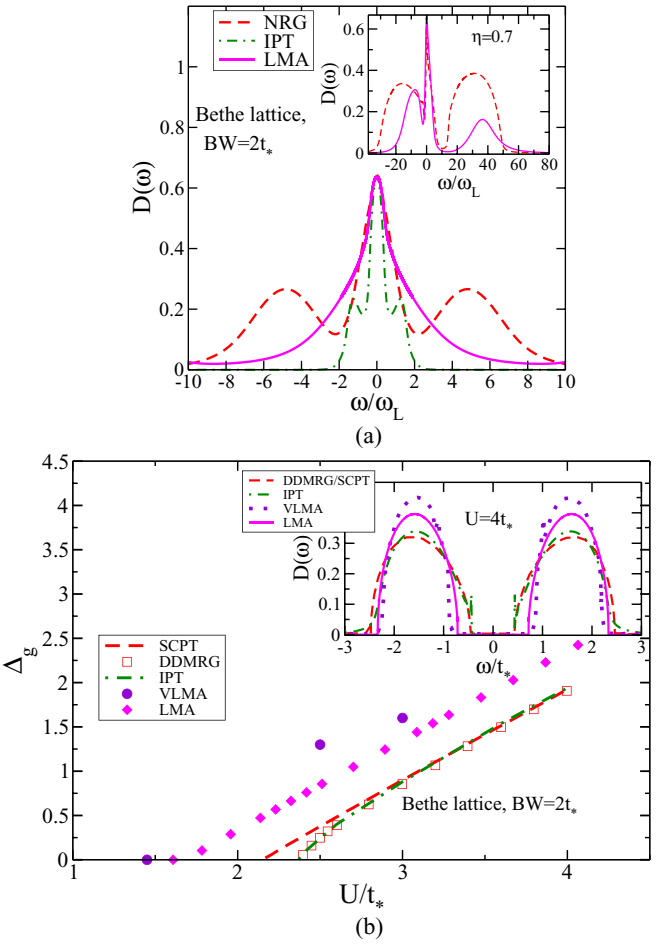

FIG. 13. (a) Scaling agreement with the NRG spectral densities. Main panel shows that at half-filling, spectral density from LMA (pink line) agrees with that from NRG (red dash) up to $\omega \sim 2\omega_L$, while IPT spectral density (green dotted dash) only agrees in the vicinity of the Fermi level. Inset shows that the agreement extends further in the p-h asymmetric case and ends near the onset of the Hubbard bands. (b) (Main) Mott gap (Δ_g) closes as the interaction strength U decreases leading to an insulator-to-metal transition at U_{c1}. U_{c1} is higher in DDMRG (Karski *et al.*), SCPT (Gebhard *et al.*), and IPT, while VLMA (Kauch and Byczuk) and LMA show $U_{c1} \simeq 1.45t_*$ and $U_{c1} \simeq 1.6t_*$, respectively. (Inset) Spectral densities as functions of frequency for various methods at $U = 4t_*$ showing Mott gaps at the Fermi level. The gaps in VLMA and LMA appear larger compared to that in DDMRG, SCPT, and IPT although the position of the Hubbard bands remain more or less the same.

V. VARIANTS OF LMA

LMA incorporates all higher order transverse spin-flip scattering or polarization diagrams in the perturbation series and hence, through DMFT, nonperturbatively captures the strong-coupling limit, e.g., $|m|$ approaching the mean-field value 1 at $U \to \infty$. However, one may investigate what happens if other kinds of diagrams are incorporated or if the RPA sum is calculated differently. For instance, Logan and his co-workers included the particle-particle and other bubble diagrams to the self-energy and found no appreciable contributions to spectral densities [31]. One can also look for another possibility, namely performing a diagrammatic sum

within GW approximation, where instead of the polarization propagator, the Coulomb interaction gets "dressed" and RPA summed [67]. However, since there are no exchange diagrams or Fock contributions considered, GW and conventional self-energies yield identical results.

Since the order of magnitude in Z does not follow many of the existing numerical results, we decide to look for open scopes where the present version of LMA can be modified. Conventional LMA uses Eq. (10) to ensure Fermi liquid properties of metallic phase and such a condition may be satisfied in various ways (e.g., Luttinger pinning, Luttinger's sum rule, variational approaches), without altering the basic physics of LMA (transverse spin-flip dynamics). This leaves open the possibility of modifying LMA from its conventional form. We discuss a few such variations that we have tested and mention their outcomes below.

A. VLMA

The VLMA is already mentioned in previous sections. Kauch and Byczuk [68] proposed that the ground state would be found through minimization of the impurity energy functional with respect to the local moment m and occupation number. For the half-filling case, only m is treated as a variational parameter. Such a variational method remains unbiased in the sense that it does not need to impose an FL condition like Eq. (10); the FL property and the Fermi level pinning is expected to be the natural outcome of the ground state, obtained through the minimization. Unlike the conventional LMA, VLMA is remarkably devoid of the low Z pathology in the former. Despite this success, the minimization procedure becomes extremely difficult at large U/t_* [68] and standard minimization routines often break down [69]. For example, we also encounter difficulties with the *golden section search method* based minimization for $U > 1t_*$. For $U = 1t_*$, we compare our spectral density to that by Kauch and Byczuk in the inset of Fig. 14 and find close agreement. Due to this subtlety associated with VLMA, we look for further alternatives which may overcome the low Z issue of the conventional LMA and discuss a few of them in the forthcoming subsections.

B. Luttinger LMA (L-LMA)

Another alternative way of bypassing Eq. (10) could be tuning m such that Luttinger's sum rule [Eq. (11)] is satisfied. For the half-filling case, satisfying the sum rule is redundant, when Fermi liquid condition is already satisfied through Eq. (10). We dub this method Luttinger LMA (L-LMA) and it shows a "sensible" Z and the quasiparticle width agrees with low U/t_* spectral density of VLMA (thick violet curve in inset of Fig. 14). Nevertheless the Luttinger pinning is missing and finding legitimate numerical solutions at higher interaction strength remains challenging. A possible remedy could be tuning occupancy or ϵ_d such that $D(0) = D_0(0)$ is satisfied (for the half-filling the solution for ϵ_d must be equal to $-U/2$), which we have not attempted yet.

C. Self-energy averaged LMA (SEA-LMA)

By construction, the spin-dependent self-energies behave like the self-energy of an FL, i.e., $\mathrm{Im}\Sigma_\sigma(\omega) \sim \omega^2$ [31] as $\omega \to 0$. We exploit this property and define an average self-energy for the paramagnetic case: $\Sigma(\omega) \equiv [\Sigma^{\mathrm{tot}}_\uparrow(\omega) + \Sigma^{\mathrm{tot}}_\downarrow(\omega)]/2$. This averaged self-energy is directly used in finding the local Green's function and through $\mathcal{G}_\sigma$ in the DMFT iteration the local moment gets updated. We name this self-energy averaged LMA (SEA-LMA). This always ensures the FL nature in the spectral density along with the Luttinger pinning since now $\mathrm{Im}\,\Sigma(\omega) \sim \omega^2$ as $\omega \to 0$ as well. The main panel in Fig. 14 shows well the agreement with the NRG spectral density in the quasiparticle regime. We also notice that at moderate U/t_*'s both NRG and SEA-LMA have almost equal values of Z (e.g., $Z \simeq 0.26$ at $U = 2t_*$). The VLMA spectral density also agrees around the Fermi level. However, VLMA and SEA-LMA show diminished and enhanced Hubbard band heights compared to that in NRG.

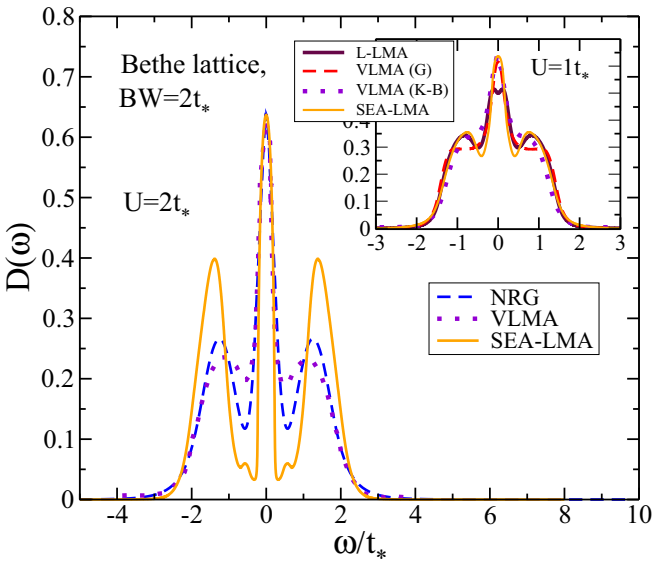

FIG. 14. (Main) Spectral densities against frequency for NRG, VLMA, and SEA-LMA at $U = 2t_*$. Although the weight of Hubbard bands differ, both VLMA and SEA-LMA show resemblance with NRG in low-energy behavior (width of quasiparticle resonance) at $U = 2t_*$. (Inset) The same at $U = 1t_*$ for Luttinger LMA (L-LMA), VLMA by golden section search (G), VLMA by Kauch and Byczuk (K-B), and SEA-LMA. All show close resemblances, however, L-LMA misses the Luttinger pinning at the Fermi level.

We must mention that a physical justification of self-energy averaging is still required and further detailed analysis is needed to be done, which is beyond the scope of this paper. As of now SEA-LMA works like another ansatz that preserves the FL property in the metallic regime.

VI. SUMMARY

In summary, we must say that, within the LMA+DMFT framework, our work investigates the unexplored part of the single orbital Hubbard model, i.e., the metallic phase at arbitrary filling and the phase diagram on the filling-interaction plane at zero temperature. LMA shows Mott MIT like many other solvers of the DMFT impurity problem. However, the transition point differs from many other methods, mainly due to the lower value of the quasiparticle residue Z (at

least by one order of magnitude). This is also what prevents LMA spectral densities from getting directly benchmarked against other numerical methods. Nevertheless we compare the spectral densities in the renormalized Fermi liquid scale ω_L and find excellent agreement with results obtained from NRG calculations for both p-h symmetric and asymmetric cases, signifying that ω_L indeed behaves like the Kondo scale, similarly found in case of LMA for the Anderson impurity model. We also propose a few possible modifications to the conventional LMA, such as variational LMA, Luttinger LMA, and self-energy averaged LMA, that remedy the low Z issue. However, these methods require systematic physical justifications and benchmarking with numerical consistency checks. If we leave this issue aside for a moment, we can see that LMA successfully captures all essential physics of the Hubbard model. For instance, the spectral density with the three-peak structure (quasiparticle resonance plus two Hubbard bands) in the metallic phase. Specifically the Luttinger pinning of the spectral density is excellently fulfilled in LMA, which is a difficult challenge for many other numerical methods. Being semianalytical, IPT and LMA both possess similar advantages, e.g., being computationally nonexpensive and capable of producing qualitatively correct physics. However, the spectral moment sum rule breaks down for IPT in the insulating regime, where LMA plays its best role. The strong-coupling universality and presence of the pseudogap may require deeper understanding in connection with the impurity model physics [35]. The optical properties also reflect universal features and a finite temperature extension to it, which in principle requires no extra formalism, could be a topic of our follow-up paper and this may attempt to find some answers to the long-lasting puzzles in experiments of doped Mott insulators [70]. Being semianalytical and hence computationally less expensive, a multiorbital extension of LMA would be an extremely powerful tool to investigate related problems.

ACKNOWLEDGMENTS

For being introduced to this interesting problem the author is grateful to N. S. Vidhyadhiraja, whose expertise in the LMA+DMFT method offered substantial help. He thanks Ralf Bulla and Anna Kauch for useful discussions and providing needful resources. He also thanks DST and DAE, Government of India, for providing financial support and scientific resources and Vikram Tripathi and Rajdeep Sensarma for their advice.

APPENDIX: ANALYTICAL DETERMINATION OF U_{c2}

Close to the MIT, singularities arise in $\Sigma(\omega)$ and $\mathcal{G}(\omega)$ and both of their positions shift to the Fermi level ($\omega = 0$) after the Mott transition. Let us assume that the poles occur at $\omega = \pm\omega_0$ in $\mathcal{G}(\omega)$ and at $\omega = \pm\omega_0'$ in $\Sigma(\omega)$, respectively, near the MIT. Then we can express the self-energy in a generic way [50,71]:

$$\Sigma(\omega) = U^2 A\left[\frac{1}{\omega-\omega_0'} + \frac{1}{\omega+\omega_0'}\right] + B\omega + C, \tag{A1}$$

where $B \equiv 1 - 1/Z$.

If we write: $\omega_0' = \beta\omega_0$, then at $\omega = \omega_0$,

$$\begin{aligned}\Sigma(\omega_0) &= U^2 A\left[\frac{1}{\omega_0(1-\beta)} + \frac{1}{\omega_0(1+\beta)}\right] + B\omega_0 + C \\ &= -\frac{U^2}{r\omega_0} + B\omega_0 + C; \end{aligned}\tag{A2}$$

$r \equiv 2A/(\beta^2 - 1)$.

Now the Dyson's equation provides

$$\begin{aligned}\Sigma(\omega_0) &= -G^{-1}(\omega_0) \\ &= -\epsilon_d - \gamma(\omega_0)\left[1 - M_2^0/\gamma^2(\omega_0)\right] \\ &= -\epsilon_d - \gamma(\omega_0) + \frac{M_2^0}{\gamma(\omega_0)} \qquad \text{(A3)} \\ &= -\epsilon_d - [\omega_0 - \epsilon_d - \Sigma(\omega_0)] + \frac{M_2^0}{\omega_0 - \epsilon_d - \Sigma(\omega_0)} \\ &= -\omega_0 + \Sigma(\omega_0) + \frac{M_2^0}{\omega_0 - \epsilon_d - \Sigma(\omega_0)}, \qquad \text{(A4)}\end{aligned}$$

where we use the fact that $\mathcal{G}_0^{-1}(\omega_0) = 0$ and $G(\omega_0) \simeq [1 + M_2^0/\gamma^2(\omega_0)]/\gamma(\omega_0)$, $M_2^0 \equiv M_2(U = 0)$ setting the chemical potential $\mu = 0$.

Equation (A4) can be reduced to a quadratic equation of ω_0,

$$\omega_0[\omega_0 - \epsilon_d - \Sigma(\omega_0)] - M_2^0 = 0\,, \tag{A5}$$

which, by using Eq. (A2), can be expressed as

$$\begin{aligned}&\omega_0^2 - \Sigma(\omega_0)\omega_0 - \epsilon_d\omega_0 - M_2^0 = 0 \\ &\Rightarrow \omega_0^2 - \left[-\frac{U^2}{r\omega_0} + B\omega_0 + C\right]\omega_0 - \epsilon_d\omega_0 - M_2^0 = 0 \\ &\Rightarrow \omega_0^2 - \left[-\frac{U^2}{r} + B\omega_0^2 + C\omega_0\right] - \epsilon_d\omega_0 - M_2^0 = 0 \\ &\Rightarrow (1-B)\omega_0^2 - (C+\epsilon_d)\omega_0 = M_2^0 - \frac{U^2}{r} \\ &\Rightarrow \frac{\omega_0^2}{Z} - (C+\epsilon_d)\omega_0 = M_2^0 - \frac{U^2}{r}. \end{aligned}\tag{A6}$$

Now ω_0 vanishes when the right-hand side of Eq. (A6) disappears at $U = U_{c2}$. (Note that the position of ω_0 decides whether Z remains finite or zero, hence $\omega_0 \to 0$ limit dominates over $Z \to 0$.) Therefore,

$$U_{c2} = \sqrt{rM_2^0}. \tag{A7}$$

From Eq. (A6) we can estimate r by plotting ω_0^2/Z against U^2 considering the fact that ω_0^2/Z remains the dominating term on the left-hand side as Z approaches zero near the transition. Thus we find $1/r = 0.069$ for the hypercubic lattice ($M_2^0 = t_*^2/2$) and $1/r = 0.08$ for the Bethe lattice of bandwidth $4t_*$ ($M_2^0 = t_*^2$) which lead to $U_{c2} = 2.69t_*$ and $U_{c2} = 3.53t_*$ respectively.

[1] J. C. Hubbard, Proc. R. Soc. London A **276**, 238 (1963).
[2] D. B. McWhan, T. M. Rice, and J. P. Remeika, Phys. Rev. Lett. **23**, 1384 (1969).
[3] J. G. Bednorz and K. A. Müller, Z. Phys. B **64**, 189 (1986).
[4] D. R. Penn, Phys. Rev. **142**, 350 (1966).
[5] J. E. Hirsch, Phys. Rev. B **31**, 4403 (1985).
[6] A. Georges, G. Kotliar, W. Krauth, and M. J. Rozenberg, Rev. Mod. Phys. **68**, 13 (1996).
[7] J. N. Zhuang, L. Wang, Z. Fang, and X. Dai, Phys. Rev. B **79**, 165114 (2009).
[8] Q. Feng, Y.-Z. Zhang, and H. O. Jeschke, Phys. Rev. B **79**, 235112 (2009).
[9] A. Georges and G. Kotliar, Phys. Rev. B **45**, 6479 (1992).
[10] A. Georges and W. Krauth, Phys. Rev. B **48**, 7167 (1993).
[11] X. Y. Zhang, M. J. Rozenberg, and G. Kotliar, Phys. Rev. Lett. **70**, 1666 (1993).
[12] M. J. Rozenberg, G. Kotliar, and X. Y. Zhang, Phys. Rev. B **49**, 10181 (1994).
[13] M. Caffarel and W. Krauth, Phys. Rev. Lett. **72**, 1545 (1994).
[14] M. Jarrell, Phys. Rev. Lett. **69**, 168 (1992).
[15] A. Georges and W. Krauth, Phys. Rev. Lett. **69**, 1240 (1992).
[16] T. Pruschke, D. L. Cox, and M. Jarrell, Phys. Rev. B **47**, 3553 (1993).
[17] R. Bulla, A. C. Hewson, and T. Pruschke, J. Phys.: Condens. Matter **10**, 8365 (1998).
[18] R. Bulla, Phys. Rev. Lett. **83**, 136 (1999).
[19] E. Y. Loh, J. E. Gubernatis, R. T. Scalettar, S. R. White, D. J. Scalapino, and R. L. Sugar, Phys. Rev. B **41**, 9301 (1990).
[20] R. Žitko and T. Pruschke, Phys. Rev. B **79**, 085106 (2009).
[21] D. J. García, K. Hallberg, and M. J. Rozenberg, Phys. Rev. Lett. **93**, 246403 (2004).
[22] S. Nishimoto, F. Gebhard, and E. Jeckelmann, J. Phys.: Condens. Matter **16**, 7063 (2004).
[23] M. Karski, C. Raas, and G. S. Uhrig, Phys. Rev. B **77**, 075116 (2008).
[24] V. Drchal, V. Janis, J. Kudrnovsky, V. S. Oudovenko, X. Dai, K. Haule, and G. Kotliar, J. Phys.: Condens. Matter **17**, 61 (2004).
[25] A. N. Rubtsov, V. V. Savkin, and A. I. Lichtenstein, Phys. Rev. B **72**, 035122 (2005).
[26] P. Werner, A. Comanac, L. dé Medici, M. Troyer, and A. J. Millis, Phys. Rev. Lett. **97**, 076405 (2006).
[27] H. Park, K. Haule, and G. Kotliar, Phys. Rev. Lett. **101**, 186403 (2008).
[28] E. Gull, A. J. Millis, A. I. Lichtenstein, A. N. Rubtsov, M. Troyer, and P. Werner, Rev. Mod. Phys. **83**, 349 (2011).
[29] G. Kotliar, S. Y. Savrasov, K. Haule, V. S. Oudovenko, O. Parcollet, and C. A. Marianetti, Rev. Mod. Phys. **78**, 865 (2006).
[30] M. Jarrell and J. E. Gubernatis, Phys. Rep. **269**, 133 (1996).
[31] D. E. Logan, M. P. Eastwood, and M. A. Tusch, J. Phys.: Condens. Matter **10**, 2673 (1998).
[32] N. L. Dickens and D. E. Logan, J. Phys.: Condens. Matter **13**, 4505 (2001).
[33] V. E. Smith, D. E. Logan, and H. R. Krishnamurthy, Eur. Phys. J. B **32**, 49 (2003).
[34] N. S. Vidhyadhiraja, V. E. Smith, and D. E. Logan, J. Phys.: Condens. Matter **15**, 4045 (2003).
[35] N. S. Vidhyadhiraja and D. E. Logan, Eur. Phys. J. B **39**, 313 (2004).
[36] N. S. Vidhyadhiraja and D. E. Logan, J. Phys.: Condens. Matter **17**, 2959 (2005).
[37] D. E. Logan and N. S. Vidhyadhiraja, J. Phys.: Condens. Matter **17**, 2935 (2005).
[38] P. Kumar and N. S. Vidhyadhiraja, J. Phys.: Condens. Matter **23**, 485601 (2011).
[39] D. E. Logan, M. P. Eastwood, and M. A. Tusch, Phys. Rev. Lett. **76**, 4785 (1996).
[40] D. E. Logan, M. P. Eastwood, and M. A. Tusch, J. Phys.: Condens. Matter **9**, 4211 (1997).
[41] A. Kauch and K. Byczuk, Physica B **407**, 209 (2012).
[42] V. M. Turkowski and J. K. Freericks, Phys. Rev. B **73**, 075108 (2006).
[43] A. Rüegg, E. Gull, G. A. Fiete, and A. J. Millis, Phys. Rev. B **87**, 075124 (2013).
[44] Y. Lu, M. Höppner, O. Gunnarsson, and M. W. Haverkort, Phys. Rev. B **90**, 085102 (2014).
[45] E. Müller-Hartmann, Z. Phys. B **74**, 507 (1989).
[46] See Eq. (60.13b) in A. L. Fetter and J. D. Walecka, *Quantum Theory of Many-particle Systems* (McGraw-Hill, New York, 1971).
[47] E. N. Economou, *Green's Functions in Quantum Physics* (Springer, Berlin, 1983).
[48] J. M. Luttinger, Phys. Rev. **119**, 1153 (1960).
[49] J. S. Langer and V. Ambegaokar, Phys. Rev. **121**, 1090 (1961).
[50] H. Barman and N. S. Vidhyadhiraja, Int. J. Mod. Phys. B **25**, 2461 (2011).
[51] D. Vollhardt, K. Held, G. Keller, R. Bulla, T. Pruschke, I. A. Nekrasov, and V. I. Anisimov, J. Phys. Soc. Jpn. **74**, 136 (2005).
[52] A. C. Hewson, *The Kondo Problem to Heavy Fermions* (Cambridge University Press, Cambridge, 1993).
[53] P. Grete, S. Schmitt, C. Raas, F. B. Anders, and G. S. Uhrig, Phys. Rev. B **84**, 205104 (2011).
[54] S. R. White, Phys. Rev. B **44**, 4670 (1991).
[55] H. Kajueter, G. Kotliar, and G. Moeller, Phys. Rev. B **53**, 16214 (1996).
[56] T. Katsufuji, Y. Okimoto, and Y. Tokura, Phys. Rev. Lett. **75**, 3497 (1995).
[57] S. Uchida, T. Ido, H. Takagi, T. Arima, Y. Tokura, and S. Tajima, Phys. Rev. B **43**, 7942 (1991).
[58] T. Arima, Y. Tokura, and S. Uchida, Phys. Rev. B **48**, 6597 (1993).
[59] Y. Tokura, Y. Okimoto, S. Yamaguchi, H. Taniguchi, T. Kimura, and H. Takagi, Phys. Rev. B **58**, R1699(R) (1998).
[60] A. Perucchi, C. Marini, M. Valentini, P. Postorino, R. Sopracase, P. Dore, P. Hansmann, O. Jepsen, G. Sangiovanni, A. Toschi, K. Held, D. Topwal, D. D. Sarma, and S. Lupi, Phys. Rev. B **80**, 073101 (2009).
[61] M. Eckstein, M. Kollar, and D. Vollhardt, J. Low Temp. Phys. **147**, 279 (2007).
[62] M. Greger, M. Kollar, and D. Vollhardt, Phys. Rev. B **87**, 195140 (2013).
[63] The NRG data are obtained from Ralf Bulla (private communication).
[64] R. Bulla, M. T. Glossop, D. E. Logan, and T. Pruschke, J. Phys.: Condens. Matter **12**, 4899 (2000).

[65] D. E. Logan and M. T. Glossop, J. Phys.: Condens. Matter **12**, 985 (2000).
[66] M. P. Eastwood, F. Gebhard, E. Kalinowski, S. Nishimoto, and R. M. Noack, Eur. Phys. J. B **35**, 155 (2003).
[67] F. Aryasetiawan and O. Gunnarsson, Rep. Prog. Phys. **61**, 237 (1998).
[68] A. Kauch and K. Byczuk, Physica B **378-380**, 297 (2006).
[69] Anna Kauch (private communication).
[70] P. A. Lee, N. Nagaosa, and X.-G. Wen, Rev. Mod. Phys. **78**, 17 (2006).
[71] M. Potthoff, Phys. Rev. B **64**, 165114 (2001).